A multidisciplinary model coupling Lattice-Boltzmann-based CFD and a Social Force Model for the simulation of pollutant dispersion in evacuation situations

Felix Marlow, Jérôme Jacob, Pierre Sagaut

A multidisciplinary model coupling Lattice-Boltzmann-based CFD and a Social Force Model for the simulation of pollutant dispersion in evacuation situations

Felix Marlow, Jérôme Jacob *, Pierre Sagaut

Aix Marseille Univ, CNRS, Centrale Marseille, M2P2 UMR 7340, Marseille, France

ARTICLE INFO

Keywords:
Indoor airflow
Pollutant dispersion
Lattice Boltzmann Method (LBM)
Actuator Line Model (ALM)
Social Force Model (SFM)
Evacuation

ABSTRACT

In closed rooms with limited convection human motion can considerably affect the airflow and thus the dispersion of pollutant. However, in Computational Fluid Dynamics (CFD) simulations on air quality and safety for human beings this effect is generally not considered, which is mainly due to a lack of a well-founded and detailed estimation of the human behavior and the high computational cost of taking into account moving objects in CFD meshes. This work addresses this issue by coupling multidisciplinary methods to allow for a more realistic simulation of pollutant dispersion by taking into account the influence of human movements. A Social Force Model predicts trajectory and speed of each person moving in a complex environment. A lattice Boltzmann-based CFD tool provides a Large Eddy Simulation of the unsteady turbulent airflow with pollutant dispersion and thermal effects. And an Actuator Line Model supplies the CFD tool with body forces that mimic the impact of moving objects on the airflow, thus, avoiding computationally expensive dynamic meshing. The capability of the coupled model is demonstrated on three realistic evacuation scenarios with various pollutant sources and a wide range of scales (dimension from 10 to 100 m, occupation from 10 to 6000 persons). The results allow to access instantaneous environmental parameters like pollutant concentration for each person during the course of the evacuation, enabling the assessment of associated health risks.

1. Introduction

The use of Computational Fluid Dynamics (CFD) is state-of-the-art in the design and the evaluation of indoor airflows in the field of HVAC (heating, ventilation and air conditioning). Including models for the dispersion of pollutants into CFD makes it a powerful tool for the assessment of air quality and safety. This offers possibilities for a wide range of applications like the investigation of health risks associated to toxic gases or contagious aerosols, the prediction of smoke distribution in fire safety or the development of ventilation concepts to reduce contaminants in clean/sterile rooms.

Recently, in the course of the COVID-19 pandemic, CFD simulations gained some special attention to study the ways of transmission of airborne contagious diseases in indoor environments. For example, Liu et al. [1] carried out a simulation of a real COVID-19 cluster in a restaurant. The speech-driven dispersion of aerosols, which can transmit diseases, was numerically investigated by Yang et al. [2]. Li et al. [3] analyzed the dispersion of cough-generated droplets in the wake of a walking person by means of CFD.

Even if most investigations of indoor airflows focus on comfort, air quality and safety for the human beings in the room, realistic full-scale applications often do not take into account how the persons affect the airflow, e.g.: [4–7]. In closed rooms however, where air velocities from ventilation or natural convection are usually smaller than $1\ \mathrm{m/s}$, human movements with walking speeds in the order of $O(1\ \mathrm{m/s})$ can have a significant impact on the airflow and turbulence properties, which in turn govern the dispersion of pollutants. And even when the persons are not moving, their body heat creates considerable heat plumes, which affect the flow and temperature field. The effect of the wake of moving persons has been demonstrated in several experimental [8–11] and numerical studies [3,12–15], some of them including thermal effects and/or pollutant dispersion.

There are two important reasons why human movement is often neglected in realistic full-scale simulations of indoor airflows. The first issue is the consideration of moving objects (like walking humans) in CFD simulations, which generally use static meshes. Dynamic meshes that adapt to the moving object are computationally very expensive and therefore prohibitive for a large number of independently moving objects. The second issue is to predict the behavior and movement patterns of many individual persons in environments with complex

* Corresponding author.
E-mail address: jerome.jacob@univ-amu.fr (J. Jacob).

geometries. The present work addresses these issues independently with approaches from different disciplines and, by coupling them to a CFD solver, develops a new generation tool for the simulation of pollutant dispersion in rooms that accounts for the interactions between physical flow phenomena and human agent behavioral and physiological features.

The first issue – the consideration of moving objects – is solved by including a wake model into an advanced lattice Boltzmann-based Large Eddy Simulation method for turbulent flow including pollutant and heat transport. An Actuator Line Model (ALM) is implemented as wake model to simulate the effect of moving persons on the airflow without dynamic meshing. The ALM is most commonly used to model the wakes of wind turbines and wind farms and is a well proven technique for this application [16–21]. However, Cao et al. [14] showed that it also can be used to model the effect of human movement on indoor particle dispersion and that it is much more efficient and yet sufficiently accurate when compared to a dynamic mesh method.

The second issue – the prediction of human agent behavior – is solved using a Social Forces Model (SFM) to predict the instantaneous position and velocity of each agent in a complex configuration, which is based on a physical representation of personal interactions with the environment. The desired direction of each agent is provided by a Fast Marching Method (FMM). The concept of the SFM was initially developed by Helbing [22] and nowadays related models are used for the planning and evaluation of pedestrian movements in public places, infrastructure or evacuation scenarios.

These sub-models (Social Force Model, lattice Boltzmann-based Large Eddy Simulation and wake model) are independently validated and coupled with each other. The resulting multidisciplinary tool is capable of the fully realistic unsteady simulation of the dispersion of an aerial toxic pollutant in an indoor environment taking into account the effect of human movements that are based on realistic crowd behavior. This enables the prediction of how much each person is exposed to the pollutant and allows for a detailed analysis of associated health risks.

The capability of the coupled model is demonstrated at three different evacuation scenarios: a meeting room, a cinema and a concert hall. These scenarios with various pollutant sources represent complex realistic environments and cover a wide range of scales with dimensions from 10 to 100 m and occupations from 10 to 6000 persons.

The paper is organized as follows. Section 2 displays the key elements of the Social Force Model for the prediction of human agent behavior along with a validation case. Also a basic physiological model is proposed to assess the exposure of each human agent to the pollutant. Section 3 is dedicated to the lattice Boltzmann-based CFD tool for the Large Eddy Simulation of the turbulent airflow including pollutant dispersion and thermal effects. Several validation cases from literature for the used methodology are discussed. The wake model to account for the physical effects of the human agents on the air flow is explained and validated in Section 4. Section 5 presents the coupling scheme of the sub-models into a multidisciplinary simulation tool. Some results obtained by the coupled model for three demonstration cases are given in Section 6. Conclusions are drawn is Section 7.

2. Human agent behavioral model

Individual human behavior is a very complex and somewhat random matter because of the lack of deterministic laws for it and the sensitivity to a huge number of personal features and external parameters, many of them escaping quantitative modeling. But in crowds the individual randomness is less dominant so that the behavior of crowds with a well-defined objective (like leaving a room) becomes predictable. In the present work a Social Force Model (SFM) is employed to simulate the evacuation of different rooms. It provides estimates of the overall evacuation time as well as individual escape routes and times. The developed SFM is validated against an evacuation exercise from literature.

A basic physiological model to assess how much each person is exposed to the pollutant is presented at the end of this section.

2.1. Social Force Model

For the simulation of the persons' positions and velocities a Social Force Model (SFM) based on the original model proposed by Helbing [22] and Helbing and Molnar [23] was implemented. A Social Force Model is a microscopic crowd dynamics model that predicts the motion of each individual in a continuous space. It is a physical representation of the persons' interaction with the environment using Newton's laws. In this approach the position $\mathbf{x}_i$ of an individual i changes in time t according to its velocity vector $\mathbf{v}_i$:

$$\frac{\mathrm{d}\mathbf{x}_i}{\mathrm{d}t} = \mathbf{v}_i \tag{1}$$

The individual's velocity is governed by a Newtonian law, which can be written as

$$m_i \frac{\mathrm{d}\mathbf{v}_i}{\mathrm{d}t} = \mathbf{F}_i \tag{2}$$

where m_i is the individual's mass. $\mathbf{F}_i$ is the sum of all forces representing the individual's interaction with its environment:

$$\mathbf{F}_i = \mathbf{F}_i^d + \sum_{j \neq i} \mathbf{F}_{ij} + \sum_W \mathbf{F}_{iW} \tag{3}$$

$\mathbf{F}_i^d$ represents the individual's will to move in a desired direction with a desired speed and is expressed as the following relaxation process

$$\mathbf{F}_i^d = m_i \frac{\mathbf{v}_i^d k_O - \mathbf{v}_i}{\tau_i} \tag{4}$$

with τ_i a relaxation time (a smaller relaxation time leads to more aggressive behavior) and $k_O(\mathbf{x}_i)$ a factor that is usually equal to 1, but $k_O < 1$ when the individual is passing an obstacle O (e.g. stairs), which results in a reduced desired speed. The desired velocity vector is $\mathbf{v}_i^d = |v_i^d| \mathbf{n}_i^d(\mathbf{x}_i)$, where $|v_i^d|$ is the individuals desired speed and $\mathbf{n}_i^d$ the unity vector of its desired direction of movement.

The desired direction $\mathbf{n}_i^d(\mathbf{x}_i)$ is calculated once at the beginning of the simulation for the entire domain using a Fast Marching Method (FMM) as described by Sethian [24] and Kimmel and Sethian [25] for solving an Eikonal equation to compute the shortest path to the nearest exit. The FMM is a method that tracks a front propagating normal to itself and starting, in the present case, from the exits of the room. This way the momentary locations of this front are isolines of the distance to the exit. The normalized spatial derivative of the distance is used as the desired direction $\mathbf{n}_i^d(\mathbf{x}_i)$ for the SFM and thus, at any location in the room, points towards the nearest exit. The FMM is solved numerically on a grid with a resolution of $\Delta x = \Delta y = 0.15$ m.

$\mathbf{F}_{ij}$ is a repulsive force to avoid getting to close to another person j. A formulation similar as Helbing et al. [26] is used:

$$\mathbf{F}_{ij} = A \exp\left[\frac{r_i + r_j - d_{ij}}{B}\right] \mathbf{n}_{ij} \theta(\phi_{ij}) + \mathbf{F}_{ij}^{contact} \tag{5}$$

Herein, r_i and r_j are the radii of the persons, which are considered as discs, d_{ij} is the distance between the persons' centers and $\mathbf{n}_{ij}$ is the normalized vector pointing from person j to i. A and B are tuning parameters of the model controlling the personal interaction strength and range. $\theta(\phi_{ij})$ introduces anisotropy taking into account that the situation in front of individual i has more impact on its behavior than the situation behind:

$$\theta(\phi_{ij}) = \begin{cases} \lambda_i + (1 - \lambda_i) \frac{1 + \cos(\phi_{ij})}{2} & \text{if } \cos(\phi_{ij}) < \cos(\phi_{max}) \\ 1 & \text{otherwise} \end{cases} \tag{6}$$

where ϕ_{ij} is the angle between the current walking direction of i and $-\mathbf{n}_{ij}$, ϕ_{max} is the maximum angle of full perception and $\lambda_i < 1$ indicates the reduced perceptiveness behind the individual.

$\mathbf{F}_{ij}^{contact}$ is a repulsive force counteracting body compression when two persons have physical body contact:

$$\mathbf{F}_{ij}^{contact} = k^{contact} \Theta\left(r_i + r_j - d_{ij}\right) \mathbf{n}_{ij} \tag{7}$$

with a large force $k^{contact}$ and the function $\Theta(z)$ that is equal to its argument z if $z \geq 0$ (body contact), otherwise 0.

$\mathbf{F}_{iW}$ is a repulsive force to avoid getting to close to walls or other obstructions W. In this work a formulation by Yu and Johansson [27] is used:

$$\mathbf{F}_{iW} = F \exp\left[-\frac{d_{iW}}{D_0} + \left(\frac{D_1}{d_{iW}}\right)^k\right] \mathbf{n}_{iW} \tag{8}$$

Originally, this formulation was proposed as a personal repulsive force for densely populated situations to model crowd turbulence. But in this work the parameters F, D_0, D_1 and k are tuned in a way that the repulsive force is small away from walls, but strongly increases very close to walls (effect of contact force). This yields good results to overcome problems where persons got stuck when passing narrow doors.

Eq. (3) to (8) can now be used to calculate the forces acting on each individual i and Eq. (1) and (2) are then solved using a forward Euler scheme:

$$\mathbf{v}_i(t + \Delta t) = \mathbf{v}_i(t) + \frac{\Delta t}{m_i}\mathbf{F}_i(t) \tag{9}$$

$$\mathbf{x}_i(t + \Delta t) = \mathbf{x}_i(t) + \mathbf{v}_i(t + \Delta t)\Delta t \tag{10}$$

Further forces can be taken into account to model more complex behaviors, but reasonable results were achieved with this basic formulation of a SFM.

2.2. Validation of the Social Force Model

To validate and calibrate the parameters of the SFM, experimental data by Klüpfel [28] is used as reference case. Klüpfel carried out an evacuation exercise of a cinema with 101 students (see Fig. 1). While the commercials were running, the movie was stopped and the students were asked to leave the cinema. At the two exits (Route A and B) cameras were installed to record the evacuation of the cinema. The evaluation of the records provided the escape times of each individual. There are some constraints that differ from a real emergency situation pointed out by Klüpfel himself and should be kept in mind:

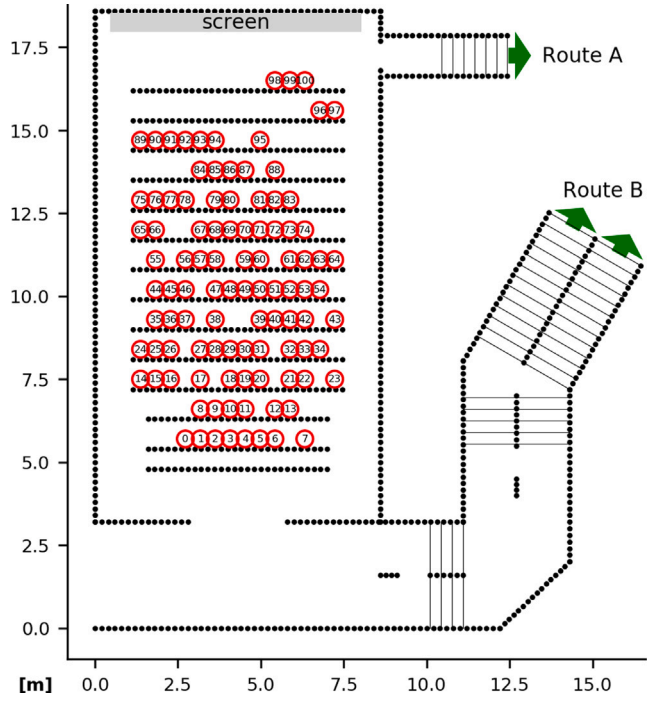

Fig. 1. Setup and occupation of the cinema in which the evacuation exercise was carried out by Klüpfel [28].

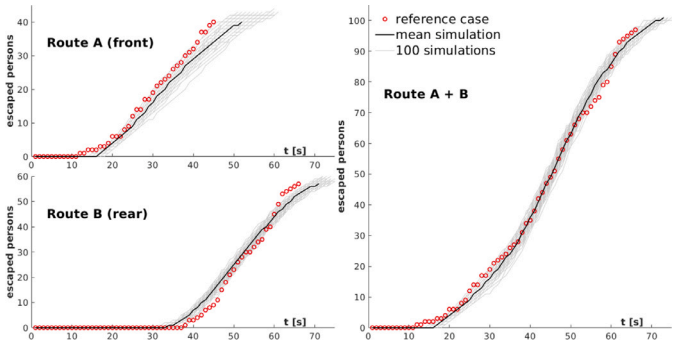

Fig. 2. Comparison of the escape times between reference case [28] and SFM.

Table 1
Calibrated parameters of the Social Force Model.

Desired velocity force $\mathbf{F}_i^d$	
Mass of a person m_i	60...100 kg
Desired speed v_i^d	1.1...1.5 m/s
Maximum speed v_i^{max}	$1.25v_i^d$
Relaxation time τ_i	0.2...0.6 s
Repulsive force between persons $\mathbf{F}_{ij}$	
A	1500 N
B	0.12 m
λ	0.5
ϕ_{max}	$\frac{5}{12}\pi$
Body contact force $\mathbf{F}_{ij}^{contact}$	
Diameter of a person r_i	0.25 m
$k^{contact}$	120000 N/m
Repulsive force of walls $\mathbf{F}_{iW}$	
F	260 N
D_0	0.2 m
D_1	0.25 m
k	15

- Students are not a representative group for an average population.
- The students were informed in advance about the procedure.
- The students were asked to act carefully to avoid injuries.

However, the evacuation exercise provides well documented empirical data of a situation similar to the cases considered in this work. Thus, the data is used as reference case for the calibration and validation of the SFM.

The parameters of the social forces were calibrated in a way to achieve a stable solution and to reproduce the escape times of the reference case. While Klüpfel [28] assumes a response time of $t_i^r = 0...4$ s (time until a person starts moving once the signal to leave the room is given), a response time of 10...14 s is used in the present work. Footage of the exercise presented on page 79 of [28] shows that at $t = 10$ s the students just got up, but hardly moved, so the response time was set accordingly.

Fig. 2 shows the number of escaped persons versus time for the reference case and the present SFM simulation. 100 simulations were carried out to show the variations resulting from the randomly generated properties of the persons (in the bounds given in Table 1). The black line shows the average of these 100 simulations. The results of the SFM agree well with the reference data, indicating that the SFM can reproduce the general phenomena occurring in the evacuation exercise and is thus capable of delivering realistic results for an evacuation situation.

Table 1 shows the final parameters of the present SFM. Some properties vary in a given range to account for differences between individuals. These varying properties are randomly generated using a truncated normal distribution in which values beyond the standard

deviation are truncated. In the simulation of the evacuation exercise two properties deviate from the values in the table to take into account the higher agility of the students compared to the average population: The desired velocity is set to $v_i^d = 1.2...1.6$ m/s and the relaxation time is set to $\tau_i = 0.1...0.5$ s. Furthermore, a response time $t_i^r = 10...14$ s is applied for the simulation of the evacuation exercise. Although this is certainly a realistic feature, a response time is not applied in the cases presented in Section 6 of this work.

2.3. Physiological model

The physiological model estimates how much each person is exposed to and affected by the pollutant. Data on the persons' positions and the instantaneous local pollutant concentration are provided by the SFM and CFD simulation, respectively. To quantify the exposure, the instantaneous pollutant concentration $\phi_i(t)$ for each person i is calculated by the inverse distance weighted average of the concentration within $r <= 0.25$ m around the person at 1.6 m above ground (head level). This yields the evolution of the momentary concentration each person is exposed to during its way through the room. Multiplication by the time step size Δt and summation over the escape time t_i^{escape} gives the total accumulated dose of pollutant a person was exposed to when it leaves the room:

$$dose_i = \sum_0^{t_i^{escape}} \phi_i(t)\Delta t \tag{11}$$

This accumulated dose can be interpreted as a measure for the skin contact of the person with pollutant (only at the head) taking into account contact concentration and duration. It is a very basic physiological model to quantify the exposure of the persons to the pollutant.

More sophisticated analyses of the physiological influence are possible, but are not presented in this work. Depending on the pollutant, a harmful dose could be defined. With that the model enables to estimate the number of harmed persons and to identify areas in which persons are particularly at risk. Taking into account only the pollutant concentrations directly in front of a person, would result in a measure for the pollution of the inhaled air. By further considering breathing rate and volume, the accumulated amount of pollutant a person inhaled could be estimated.

3. Computational fluid dynamics via lattice Boltzmann method

This section gives a brief description of the lattice Boltzmann method (LBM), which is used in this work for the Large Eddy Simulation (LES) of the unsteady turbulent airflow, and the sub-models for heat and pollutant. The validity of the specific method is shown on the basis of studies from literature that use the same method.

The LBM and the wake model (see Section 4) are implemented in a research version of the lattice Boltzmann solver ProLB (CS [29]) using a 3D lattice with 19 discrete velocities (D3Q19).

For a detailed introduction to the fundamental theory of the LBM and its application it is referred to the book by Krüger et al. [30].

3.1. Lattice Boltzmann method

The lattice Boltzmann method is based on the kinetic Boltzmann equation, i.e. the transport equation of probability distribution functions (PDFs) $f = f(t, \mathbf{x}, \mathbf{c})$. The PDFs describe the probability of encountering a particle with velocity $\mathbf{c}$ at time t at location $\mathbf{x}$, thereby providing a mesoscopic description of the fluid flow. Macroscopic quantities like velocity and density thus need to be reconstructed by relating the Boltzmann equation to the Navier–Stokes equation, which is usually done by means of the Chapman–Enskog analysis. More precisely, macroscopic quantities are reconstructed by computing the moments of $\mathbf{x}$ in the velocity space.

Discretization of the kinetic Boltzmann equation in time, space and a finite set i of discrete velocities $\mathbf{c}_i$ (the so called lattice) results in the lattice Boltzmann equation, which, in presence of a force term F_i, can be written as the following advection-relaxation equation:

$$f_i(t + \Delta t, \mathbf{x} + \mathbf{c}_i\Delta t) - f_i(t, \mathbf{x}) = \Omega_i + (1 - \frac{1}{2\tau})\Delta t F_i(t, \mathbf{x}) \tag{12}$$

The collision operator Ω_i represents the redistribution of f_i through particle collisions. The simplest collision operator is the Bhatnagar–Gross–Krook model (BGK), which models the collision process as a relaxation of the PDFs towards an equilibrium state f_i^{eq} using a single relaxation time τ:

$$\Omega_i = -\frac{1}{\tau}(f_i - f_i^{eq}) \tag{13}$$

The relaxation time towards the equilibrium is related to the molecular kinematic viscosity of the fluid ν via $\tau = \frac{\nu}{c_s^2} + \frac{\Delta t}{2}$. The time step size Δt is determined by the mesh resolution Δx and the lattice speed of sound c_s by $\Delta t = \frac{1}{\sqrt{3}}\frac{\Delta x}{c_s}$. c_s does not necessarily need to be the physical speed of sound, but can be chosen a smaller value to avoid too small time steps, as long as the simulated velocities do not exceed $|\mathbf{u}| < 0.2c_s$ [30].

The Maxwell–Boltzmann equilibrium expanded in Hermite polynomials is given by

$$f_i^{eq} = w_i\rho\left(1 + \frac{\mathbf{u}\cdot\mathbf{c}_i}{c_s^2} + \frac{1}{2c_s^4}\mathbf{H}_i^{(2)} : \mathbf{uu}\right) \tag{14}$$

where w_i are weighing factors depending to the used lattice and the second order Hermite polynomial is

$$\mathbf{H}_i^{(2)} = \mathbf{c}_i\mathbf{c}_i - c_s^2\mathbf{I} \tag{15}$$

with the identity matrix $\mathbf{I}$.

External volumic forces, namely gravity and the wake model in the present simulations, are expressed as body forces $\mathbf{f}$. Guo et al. [31] showed that, in order to match the Navier–Stokes equations, the lattice forces F_i are related to the body force $\mathbf{f}$ as

$$F_i = w_i\left[\frac{\mathbf{c}_i - \mathbf{u}}{c_s^2} + \frac{(\mathbf{c}_i\cdot\mathbf{u})}{c_s^4}\mathbf{c}_i\right]\cdot\mathbf{f} \tag{16}$$

and that the macroscopic quantities fluid density ρ and momentum $\rho\mathbf{u}$ must be reconstructed from the moments of the PDFs as

$$\rho = \sum_i f_i \tag{17}$$

$$\rho\mathbf{u} = \sum_i \mathbf{c}_i f_i + \frac{\Delta t}{2}\mathbf{f} \tag{18}$$

The solution of Eq. (12) can then be obtained thanks to a two-step Strang-like splitting method. First the collision step $f_i^{coll}(t, \mathbf{x}) = f_i(t, \mathbf{x}) + \Omega(t, \mathbf{x}) + (1 - \frac{1}{2\tau})\Delta t F_i(t, \mathbf{x})$ is solved, then, in the propagation (or streaming) step $f_i(t + \Delta t, \mathbf{x} + \mathbf{c}_i\Delta t) = f_i^{coll}(t, \mathbf{x})$ the post-collision distributions are advected to the adjacent lattice nodes.

Solving the collision operator in Eq. (13) with the original BGK model is unstable for most practical applications. Thus, the hybrid recursive regularized (HRR) BGK model presented by Jacob et al. [32] is used in this work and the lattice Boltzmann equation (12) is rewritten as (Feng et al. [33])

$$f_i(t + \Delta t, \mathbf{x} + \mathbf{c}_i\Delta t) = f_i^{eq}(t, \mathbf{x}) + (1 - \frac{1}{\tau})f_i^{neq}(t, \mathbf{x}) + \frac{\Delta t}{2}F_i(t, \mathbf{x}) \tag{19}$$

with the non-equilibrium distribution $f^{neq} = f_i - f_i^{eq} + \frac{\Delta t}{2}F_i$.

The HRR-BGK model provides a more stable and accurate solution for the collision process by a hybrid recursive reconstruction procedure for the non-equilibrium distribution f^{neq}. The non-equilibrium distribution can either be computed from the PDFs by expansion in Hermite polynomials:

$$f_i^{neq,PDF} = w_i\left(\frac{1}{2c_s^4}\mathbf{H}_i^{(2)} : \mathbf{a}^{(2),neq}\right) \tag{20}$$

with

$$\mathbf{a}^{(2),neq} = \sum_i \mathbf{H}_i^{(2)}(f_i - f_i^{eq} + \frac{\Delta t}{2} F_i) \tag{21}$$

or, following the Chapman–Enskog expansion, the non-equilibrium distribution can be approximated from the derivatives of the macroscopic velocities

$$f_i^{neq,macro} = -\frac{\tau \rho w_i}{c_s^2} \mathbf{H}_i^{(2)} : \mathbf{S} \tag{22}$$

where $\mathbf{S} = \frac{1}{2}(\nabla \mathbf{u} + (\nabla \mathbf{u})^T)$ is the strain rate tensor.

Using only $f_i^{neq,PDF}$ can lead to numerical instability, whereas considering only $f_i^{neq,macro}$ can lead to strong numerical dissipation. To avoid these problems, the two are blended:

$$f_i^{neq} = \sigma f_i^{neq,PDF} + (1-\sigma) f_i^{neq,macro} \tag{23}$$

with $0 \leq \sigma \leq 1$. When $\sigma < 1$, an artificial hyperviscosity is added to stabilize the solution.

The weighting parameter $\sigma(t, \mathbf{x})$ is dynamically tuned at each grid point and each time step in a way that the σ-induced dissipation recovers exactly the one provided by a LES subgrid scale model, thus, mimicking the effect of the sub-grid scales on the flow:

$$\sigma = \frac{1}{6\nu_t \frac{L_{VK}^2}{\Delta x^2 c_s^2 \tau} + 1} \tag{24}$$

where $L_{VK} = \frac{|\nabla \mathbf{u}|}{|\nabla^2 \mathbf{u}|}$ and ν_t is the turbulent kinematic viscosity predicted by Vreman's subgrid scale model.

Actually, the equilibrium distribution f^{eq} in Eq. (14) and the non-equilibrium distribution $f^{neq,PDF}$ in Eq. (20) are expanded in lengthy third order Hermite polynomials where only combinations with correct orthogonality properties are used. For the sake of brevity, the above equations are only written to the second order. For a detailed description of the third order Hermite polynomials and the HRR-BGK model it is referred to Jacob et al. [32] and Feng et al. [33].

3.2. Scalar transport for heat and pollutant

To account for thermal effects (for example created by the persons' body heat) and to simulate the dispersion of a pollutant, scalar transport equations for heat and pollutant are solved. Heat and pollutant transport are both modeled using the convection–diffusion equation, which, for a generic scalar Φ, assuming incompressible flow, can be written as

$$\frac{\partial \Phi}{\partial t} = -\mathbf{u}_i \frac{\partial \Phi}{\partial x_i} + D \frac{\partial^2 \Phi}{\partial x_i \partial x_i} + R \tag{25}$$

For heat transport Φ is replaced by the temperature T, R is a heat source term Q_T and the diffusivity D is

$$D_{thermal} = \alpha + \frac{\nu_t}{Pr_t} \tag{26}$$

with the molecular thermal diffusivity α, the turbulent kinematic viscosity ν_t and the turbulent Prandtl number Pr_t.

For pollutant transport Φ is replaced by the pollutant mass fraction ϕ, R is the pollutant source term S_ϕ and the diffusivity D is

$$D_{pollutant} = D_\phi + \frac{\nu_t}{Sc_t} \tag{27}$$

with the molecular mass diffusivity D_ϕ of the pollutant and the turbulent Schmidt number Sc_t.

The transport equations for heat and pollutant are not solved by LBM, but by finite differences. While the temperature affects the flow field via density differences considered by the Boussinesq approximation, the pollutant is assumed a passive gas and has no effect on the flow field.

3.3. Validation of the CFD solver

The accuracy of LBM-Large Eddy Simulations using the HRR-BGK model with force terms, which is used in the present work, has been proven in a couple of publications, including complex geometries and pollutant dispersion.

The HRR-BGK model with dynamic σ, which is used in this work, was presented by Jacob et al. [32]. A simple test case with a flow around a cylinder showed very good agreement with measurements and other well established numerical methods. Jacob and Sagaut [34] evaluated the method on a test case with a complex urban geometry aiming on pedestrian wind comfort assessment. Reference data is provided by the Architectural Institute of Japan (AIJ) open database and consists of field and wind tunnel measurements of wind velocities in the Shinjuku area in Tokyo, which contains small and large buildings. Simulation results are in good agreement with the measurements when using an appropriate mesh resolution.

Feng et al. [33] used the HRR-BGK model with force terms and the Boussinesq approximation to simulate buoyancy effects by temperature and humidity differences, where the scalar transport of temperature and humidity are solved by the finite volume method. A similar method is used in the present work to take into account thermal effects, while humidity is not considered. Feng et al. [33] proved the validity of the method by achieving excellent agreement of their simulations with numerical benchmark solutions of a 2D Rayleigh–Bénard convection and other more complex atmospheric convection problems.

Simulations of urban flows with pollutant dispersion are compared to reference cases by Merlier et al. [35,36]. Both papers use basically the same implementation as the present paper with the HRR-BGK model and scalar transport of pollutant solved by finite differences. In [35] simulation results are compared to wind tunnel measurements from the CODASC benchmark (COncentration DAta of Street Canyons). A simplified street canyon with a pollutant source at the bottom of the canyon under perpendicular wind conditions was investigated. The simulations showed good agreement of pollutant concentrations at the leeward wall, but some differences at the windward wall and, in that, performed as good as other state-of-the-art simulations for the same benchmark. In [36] simulation results are compared to wind tunnel measurements from the MODITIC project (MOdeling the DIspersion of Toxic Industrial Chemicals in urban environments). A central Paris area with a complex street network was investigated with different pollutant sources and wind directions. Good agreement with the complex pollutant concentration distributions and their fluctuations were achieved by the simulations.

4. Wake model of the human agents

A person moving through a room is dragging air in its wake, disturbs the surrounding airflow and creates turbulence. To be able to model the influence of moving persons on the airflow without moving mesh boundaries and in rooms with different scales of size and mesh resolution, the Actuator Line Model (ALM) is used as wake model. The ability of the model to reproduce the wake and its effect on the dispersion of pollutant is shown.

For the sake of simplicity, persons are represented by cylinders with a height of $H = 1.8$ m and a radius of $R = 0.25$ m.

4.1. Actuator Line Model

The Actuator Line Model is based on the idea that the drag force experienced by a body moving through a fluid equals the forces that cause the flow disturbances. Hence, the effect of the moving body on the fluid can be modeled by applying the reverse drag force as a body force to the fluid.

The drag force of a body can be computed by the drag equation:

$$\mathbf{F}_D = \frac{1}{2} \rho A C_D \mathbf{u}_{rel} |\mathbf{u}_{rel}| \tag{28}$$

where ρ is the fluid density, C_D is the drag coefficient, $\mathbf{u}_{rel} = \mathbf{u}_\infty - \mathbf{u}_s$ is the difference between free stream velocity $\mathbf{u}_\infty$ and the velocity of the moving body $\mathbf{u}_s$ and $A = 2RH$ is the projected cross sectional area of the body.

The drag coefficient of an infinite cylinder in a flow perpendicular to its axis is $C_D \approx 1.2$ for Reynolds numbers between $10^4 < Re < 10^5$ [37], which, with the present parameters, corresponds to approximately $0.3 < u < 3$ m/s. Tip effects at the end of the cylinder (the person's head) on the drag coefficient are ignored. Furthermore, only the horizontal x- and y-components of the velocity are taken into account, neglecting vertical movement and flow, which ought to be small compared to the horizontal components.

Each cylinder (or person) is modeled by an actuator line located at the cylinder axis. The actuator line is divided into a number of segments to allow for a variation of the force along the actuator line. For each segment a drag force is computed, which is reversely applied to the fluid at the center of the segment:

$$\mathbf{F}_{seg} = -\mathbf{F}_{D,seg} = -\frac{1}{2}\rho C_D \mathbf{u}_{rel}|\mathbf{u}_{rel}|2RH_{seg} \tag{29}$$

For numerical stability these punctual forces at the segment centers are smeared over a volume (thus applied to several lattice nodes) using a normalized 3D Gaussian kernel:

$$g(r) = \frac{1}{(\epsilon\sqrt{\pi})^3}\exp\left(-\frac{r^2}{\epsilon^2}\right) \tag{30}$$

with r the distance between the lattice node and the center of the segment and ϵ the Gaussian width, which is set to $\epsilon = 0.2$ m in this work (for details on the choice of ϵ see Section 4.2).

Summation over all segments finally yields the body force at each lattice node

$$\mathbf{f} = \sum_{seg} \mathbf{F}_{seg} g(r_{seg}) \tag{31}$$

which is applied to the lattice Boltzmann equation by insertion into Eq. (16).

The free stream velocity $\mathbf{u}_\infty$ used to calculate $\mathbf{u}_{rel} = \mathbf{u}_\infty - \mathbf{u}_s$ in Eq. (29) is estimated from the local velocity at each segment center $\mathbf{u}_{seg}$ using the estimation provided by Martínez-Tossas et al. [38]:

$$\mathbf{u}_\infty = \frac{\mathbf{u}_{seg}}{1 - \frac{1}{4\sqrt{\pi}} C_D \frac{2R}{\epsilon}} \tag{32}$$

This estimation is necessary because the drag coefficient in Eq. (28) is based on the undisturbed free stream velocity $\mathbf{u}_\infty$, but the velocity sampled at the segment center $\mathbf{u}_{seg}$ is affected by the applied actuator line forces $\mathbf{f}$.

Wake interactions (when a person is passing the wake of another person) are taken into account by the ALM because $\mathbf{u}_{rel} = \mathbf{u}_\infty(\mathbf{u}_{seg}) - \mathbf{u}_s$ used to calculate the wake forces is based on the local fluid velocity $\mathbf{u}_{seg}$ at the person's position.

The height of a segment is set to $H_{seg} = \epsilon$, which is the upper limit to ensure a smooth force distribution over the length of the actuator line.

To account for the human body heat, each person is considered a heat source with a power of $P = 80$ W. This power is distributed over the segments of the actuator line and spread over several mesh nodes using the Gaussian kernel from Eq. (30). This yields the following thermal source term, which is added to the thermal transport equation (25)

$$Q_T = \sum_{seg} \frac{P}{\rho c_p} \frac{H_{seg}}{H} g(r_{seg}) \tag{33}$$

where c_p is the specific heat capacity of the fluid.

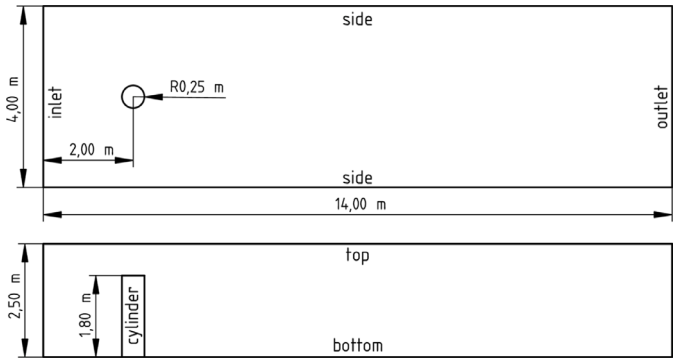

Fig. 3. Test case setup.

4.2. Validation of the wake model

The ALM is widely used and well proven to model the wake of wind turbines and wind farms. There are numerous publications validating the ALM in the Navier–Stokes framework against measurements or less simplified CFD simulations [17–19,39], but it has been successfully applied in the lattice Boltzmann framework as well [20,21,40]. The validity of the method to model the impact of human movement on the particle dispersion in rooms was shown by Cao et al. [14].

In the present application the wake model is primarily meant to take into account the effect of moving persons on the airflow and the distribution of pollutant. For that reason, the validation of the wake model is done rather on a qualitative base.

The reference case is a CFD simulation with the same LBM solver as described in Section 3.1 of a flow around a cylinder where the cylinder is resolved in the mesh. The domain is a rectangular channel, 14 m long, 4 m wide and 2.5 m high (see Fig. 3). The upright cylinder is standing on the bottom and has a height of $H = 1.8$ m and a radius of $R = 0.25$ m (same dimensions as used in the demonstration cases in Section 6 where the cylinders, i.e. moving persons, are modeled by the ALM). The mesh is a Cartesian grid with a resolution of $\Delta x = 0.02$ m. At the inlet a uniform velocity of $u_\infty = 1.5$ m/s is specified, at the outlet a constant pressure. While the cylinder is fixed with no-slip boundary condition, the bottom and top are modeled as no-slip walls that are moving with the inlet velocity. The sides are defined as free-slip walls. The setup is thus similar to a cylinder moving through a stagnant fluid.

The results of this simulation with resolved cylinder are used as reference case to demonstrate the validity of the wake model. Simulations with the wake model are carried out in the same domain, but the cylinder is modeled by the ALM instead of being resolved in the mesh. Three different mesh resolutions are tested with the ALM that correspond to the resolutions in the three demonstration cases presented in Section 6: $\Delta x = 0.02$ m, $\Delta x = 0.10$ m and $\Delta x = 0.20$ m.

There are different recommendations for the choice of the Gaussian width ϵ in literature. Most of these recommendations are for the application of wind turbines, so they are related to the blade chord length c as geometric length scale, which corresponds to the diameter of the cylinder $2R = 0.5$ m in the present work. The recommendations relevant for the present work are listed in Table 2. Churchfield et al. [18] recommend that the applied forces are concentrated within the modeled geometry to ensure physical similarity. The Gaussian function $g(r)$ in Eq. (30) decreases to 1% of its maximum at $r = 2.15\epsilon$, which yields $\epsilon_{rec} = \frac{c}{4.3} = \frac{2R}{4.3} \approx 0.12$ m. A similar optimal value was found by Martínez-Tossas et al. [38] with $\epsilon_{rec} \approx \frac{c}{5}$. Several authors [17,18,41] found a limit of $\epsilon_{rec} \geq 2\Delta x$ to ensure numerical stability in the Navier–Stokes framework. Similar values for the limit between $1\Delta x < \epsilon_{min} < 2\Delta x$ where found with the present model in the LBM framework. Martínez-Tossas et al. [38] empirically found that the estimation of the free stream velocity in Eq. (32) is accurate at least

Table 2
Recommendations for the Gaussian width ϵ.

With: $c = 2R = 0.5$ m, $\Delta x = 0.1$ m[a], $C_D = 1.2$		
Criteria	Recommendation	ϵ_{rec}
Physical similarity [18,38]	$\epsilon = \frac{c}{4.3}$	$\epsilon \approx 0.12$ m
Numerical stability [17,18,41]	$\epsilon \geq 2\Delta x$	$\epsilon \geq 0.20$ m[a]
Estimation of u_∞ [38]	$\frac{1}{4\sqrt{\pi}} C_D \frac{c}{\epsilon} \leq 0.28$	$\epsilon \geq 0.30$ m

[a]Exemplary; mesh resolution is case dependent.

up to $\frac{1}{4\sqrt{\pi}} C_D \frac{c}{\epsilon} \leq 0.28$, which yields $\epsilon_{rec} \geq 0.3$ m with the parameters in the present work.

As seen in Table 2 some of the recommendations are in conflict with each other. In the present work a Gaussian width of $\epsilon = 0.2$ m was found to be a suitable value, which was used for all cases, regardless of the mesh resolution. With this value a good reproduction of the wake is achieved and it is stable even on the coarsest mesh with $\Delta x = 0.20$ m.

Fig. 4 shows the time averaged velocity field of the wake for the reference case and the three different meshes using the ALM as wake model. The velocity is shown in a horizontal plane at half cylinder height at $z = H/2 = 0.9$ m and is normalized with the inlet velocity u_∞. The ALM reproduces the wake structure of the reference case (Fig. 4(a)) quite well on the meshes with $\Delta x = 0.02$ m (Fig. 4(b)) and $\Delta x = 0.10$ m (Fig. 4(c)). The lack of sharp velocity gradients at the cylinder, as a result of the smoothing of the actuator forces, leads to a difference in the recirculation zone, but the dynamics of the wake with vortex shedding are captured, resulting in a V-shaped wake. However, on the coarsest mesh with $\Delta x = 0.20$ m (Fig. 4(d)) the large ratio $\frac{\Delta x}{\epsilon}$ reduces the steep gradients at the flanks of the Gaussian and turbulent structures are filtered by the LES so that no vortex shedding is triggered. Nevertheless, the momentum applied to the flow is similar as in the reference and the other ALM cases. Furthermore, Troldborg et al. [39] showed that the wake created by the ALM breaks up faster when using turbulent inflow instead of uniform inflow (as in the present test case) and as a result compares much better to simulations with mesh resolved geometry. This indicates that in realistic scenarios, where the ambient air is likely to be turbulent due to room ventilation, convection and wake interactions, the ALM can reproduce wakes even better than in the present test case.

The effect on the pollutant dispersion is demonstrated in the same simulation of the cylinder flow. Once the flow field is fully established, the pollutant concentration in the incoming air is set to a constant value during one second. The pollutant cloud is convecting through the domain, thus, the passing of the cylinder through a pollutant cloud is simulated. Fig. 5 shows the instantaneous pollutant concentration 5 s after the cylinder passed the core of the pollutant cloud. The concentration is shown in a horizontal plane at half cylinder height at $z = H/2 = 0.9$ m and is normalized with the incoming concentration ϕ_{max}. The fine turbulent structures originating from the sharp shear layer and separation at the cylinder surface, which can be seen in the reference case (Fig. 5(a)), are not reproduced by the ALM (Fig. 5(b) to Fig. 5(d)). Nevertheless, the entrainment of pollutant in the cylinder wake, which is the phenomenon of interest in this work in order to investigate pollutant dispersion under the influence of human movements, is captured by the ALM. And as mentioned before, the ALM can be expected to produce a more turbulent wake when applied to realistic indoor flows with turbulent ambient air.

For a quantitative analysis of the pollutant entrainment in the wake, the domain was subdivided along the x-axis (flow direction) into slices of one meter thickness. Fig. 5(e) shows the mean pollutant concentration within each slice normalized with the incoming concentration. For example, the value at $x = 1$ m is the average between $0.5 < x < 1.5$ m (bounds indicated by white lines). On the same mesh as the reference

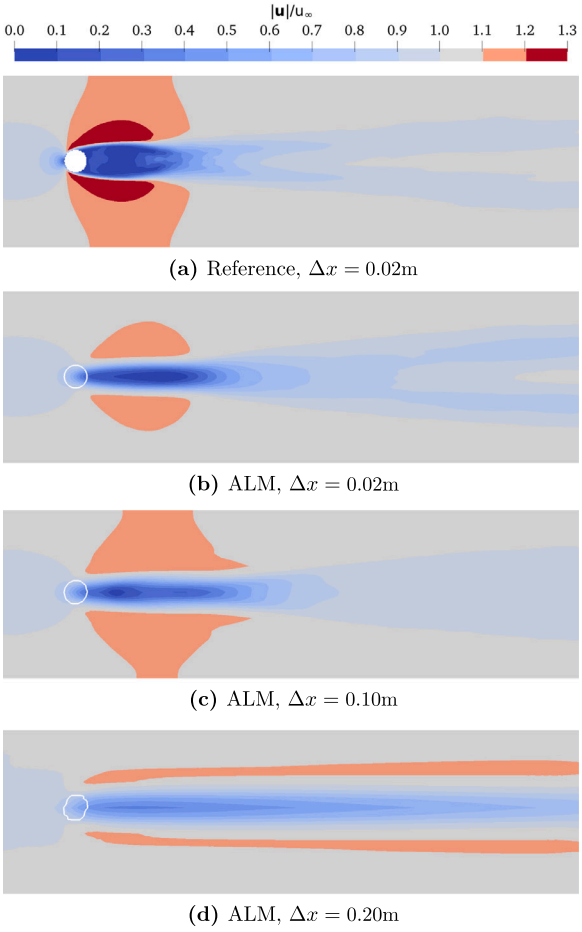

Fig. 4. Time averaged velocity field around a cylinder at $z = H/2 = 0.9$ m. (For interpretation of the references to color in this figure legend, the reader is referred to the web version of this article.)

case ($\Delta x = 0.02$ m) the ALM matches the mean pollutant concentrations along the wake very well. Only directly behind the cylinder the concentration is underestimated because the recirculation zone cannot be accurately reproduced by the ALM. Still a good agreement is achieved on a much coarser mesh ($\Delta x = 0.10$ m) with the ALM. A significant deviation from the reference case can be seen with the ALM and $\Delta x = 0.20$ m, the case in which the wake dynamic is not captured. Considering the abstraction of the cylinder by the ALM, the very coarse mesh and the uniform inflow, the results are nevertheless acceptable in order to estimate the effect of moving persons on the pollutant dispersion in rooms.

5. Coupling

Several sub-models to account for different aspects of pollutant dispersion in rooms and the effect of humans on it has been explained:

- **Social Force Model** (SFM) and **Fast Marching Method** (FMM): Simulation of the positions and velocities of persons moving in a room (Section 2.1)
- **Lattice Boltzmann method** (LBM): Large Eddy Simulation of the airflow in the room (Section 3.1)
- **Scalar transport equation for heat**: Account for heat production of the human body and its thermal effects on airflow (Section 3.2)
- **Scalar transport equation for pollutant**: Account for pollutant dispersion in the room (Section 3.2)
- **Wake model**: Account for the effect of human movements on the airflow (Section 4)

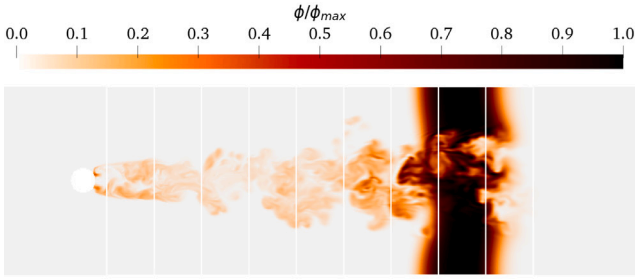

(a) Reference, $\Delta x = 0.02$m

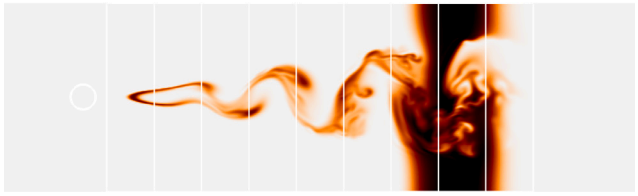

(b) ALM, $\Delta x = 0.02$m

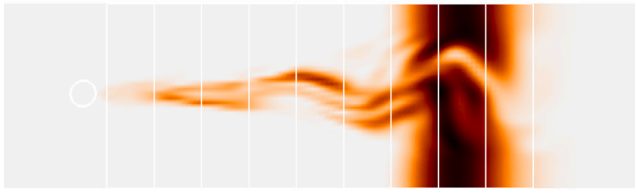

(c) ALM, $\Delta x = 0.10$m

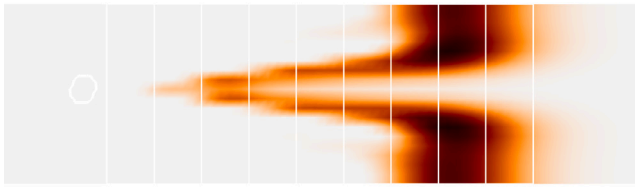

(d) ALM, $\Delta x = 0.20$m

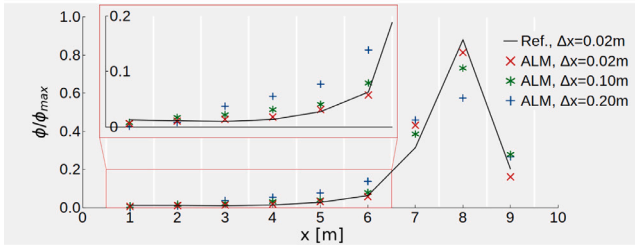

(e) Pollutant concentration along the x-axis averaged over 1m slices.

Fig. 5. Pollutant concentration 5 s after the cylinder passed the core of the pollutant cloud. (For interpretation of the references to color in this figure legend, the reader is referred to the web version of this article.)

- **Physiological model**: Analysis of the exposure of the persons to pollutant (Section 2.3)

For a most realistic simulation of the dispersion of pollutant in a room with moving persons the above sub-models are coupled with each other. Due to a lack of adequate and reproducible reference data for pollutant dispersion with large-scale human movements in complex environments, it is not possible to validate the accuracy of the coupled model. Instead the sub-models were validated separately (see corresponding sections) and the strongest interactions between the sub-models are taken into account by the coupling scheme, which is shown in Fig. 6.

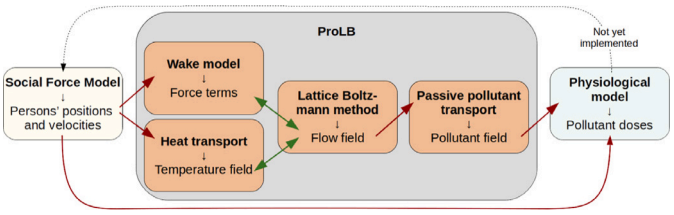

Fig. 6. Coupling scheme of the sub-models.

Table 3
Overview of the simulated cases.

Case	L_{max}	n_p	Pollutant source
Meeting room	8 m	10	Through ventilation inlets
Cinema	28 m	336	Release from a jet
Concert hall	83 m	6026	Initial cloud

The SFM is a stand-alone application providing the positions and velocities of all the persons moving in a room. It is thus easily possible to use a more advanced or specific behavioral model that provides these information instead of the SFM presented in Section 2.1.

The data on the human movement is fed as input into the wake model (uses persons' positions and velocities) to calculate the force terms modeling the effect of the moving persons and into the heat transport equation (uses persons' positions only) to account for the heat production of the human body. The force terms from the wake model and the temperature field from the heat transport equation are each two-way coupled with the flow field, which is simulated by the lattice Boltzmann method. The force terms are explicitly considered in the lattice Boltzmann equation and the temperature field is directly influenced by the flow field while it affects the flow field via the Boussinesq approximation. The flow field governs the pollutant transport equation to solve the pollutant dispersion, which is considered passive and has thus no effect on the flow field. The Lattice Boltzmann method, the transport equations for heat and pollutant and the wake model are implemented into the ProLB solver.

The pollutant field in conjunction with the persons' positions is fed as input data into the physiological model to estimate the pollutant dose each person is exposed to. With appropriate models for the effect of particular pollutants on the human physiology this information could be fed back into the SFM to affect the individual performance of the persons, but this is not done in the current work.

6. Demonstration of the coupled model

The capability of the coupled model is demonstrated considering three cases covering a wide range of room size and occupation. In all three cases a pollutant is released into the room (via different source types) and the evacuation of the room is simulated. Table 3 gives an overview of the three cases indicating the maximal extent of the room L_{max}, the number of persons in the room n_p and how pollutant is released into the room.

In the following results the pollutant concentrations ϕ are normalized with the inlet or initial pollutant concentration ϕ_{max}. The accumulated doses of pollutant $dose_i$, determined by the physiological model (see Section 2.3), are normalized with the highest dose received by a person in the respective scenario $dose_{max}$.

6.1. Meeting room

This case is a meeting room ($8.2 \times 4.3 \times 2.5$ m) with a door leading to a corridor with one exit (see Fig. 7). 10 persons are initially located around an oval table. Pollutant is released within the airflow though the ventilation inlets in the ceiling. The evacuation starts 60 s after the

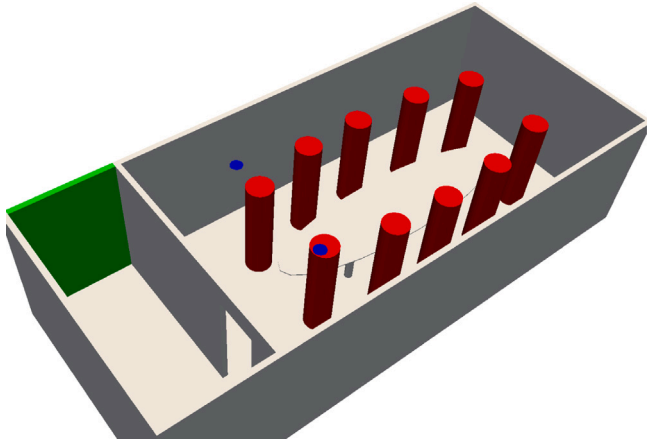

Fig. 7. The meeting room with initial position of the persons (red), exit (green) and ventilation inlets in the ceiling (blue) through which the pollutant is released. (For interpretation of the references to color in this figure legend, the reader is referred to the web version of this article.)

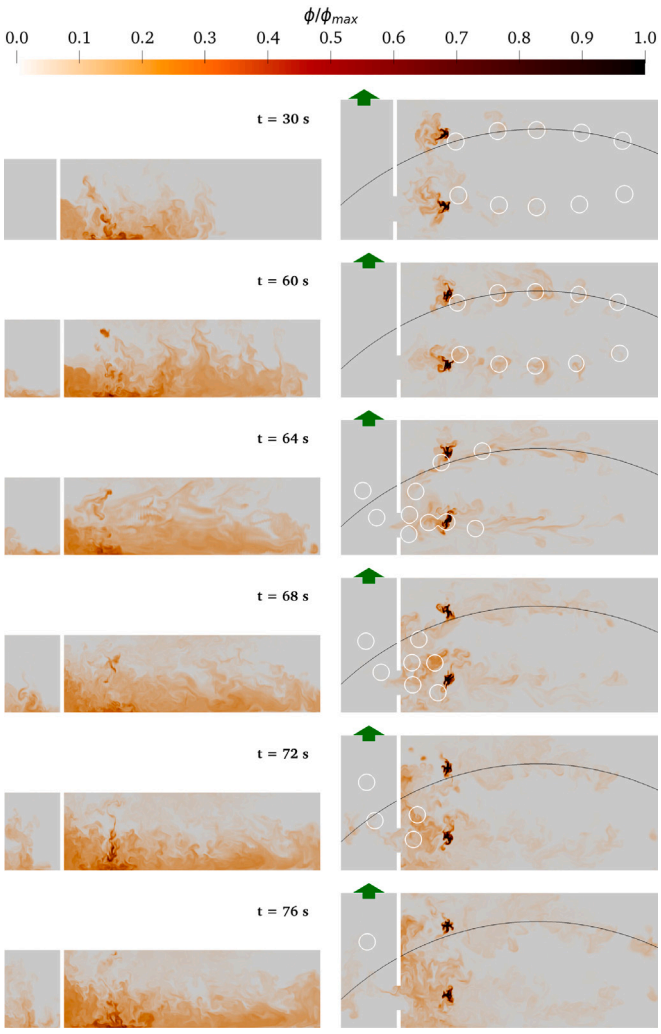

Fig. 8. Meeting room: pollutant concentration in curved vertical plane (left) and at head level (right, white lines indicate position of persons, black line indicates location of vertical plane).

beginning of the pollutant release and it takes 17.1 s for all persons to leave via the corridor.

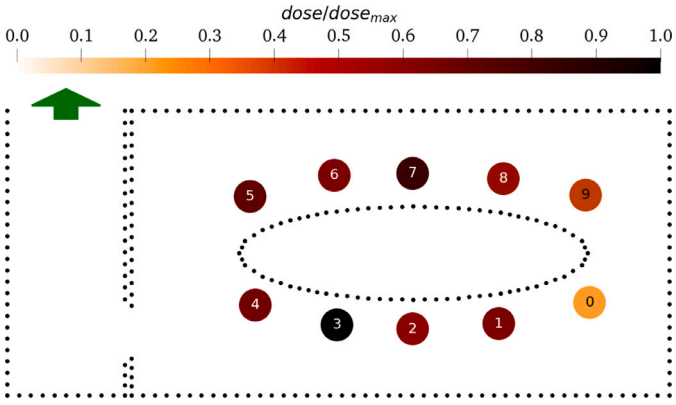

Fig. 9. Meeting room: the accumulated dose of pollutant that each person is exposed to plotted on their initial position.

The mesh is a Cartesian grid with a resolution of $\Delta x = 0.02$ m in the entire domain, resulting in 14.5 million nodes.

The instantaneous distribution of the pollutant in the meeting room is shown in Fig. 8 for several time steps. The white lines on the right side are iso-lines of the Gaussian kernel to indicate the position of the persons (for this reason multiple persons appear to merge in densely populated areas). Before the persons start moving at $t = 60$ s, pollutant is mostly concentrated near the ground and is advancing from the ventilation inlets into the room (see first two time steps in Fig. 8). The pollutant sinks to the ground because it is released within the airflow from the ventilation inlets, which is colder and has thus a higher density. The body heat of the motionless persons creates heat plumes in which air with higher pollutant concentration rises and reaches head level. As soon as the persons start moving, mixing caused by the persons' wakes takes over and air with high pollutant concentrations is drawn towards the door and finally out into the corridor.

Fig. 9 shows the accumulated dose of pollutant that each person was exposed to when leaving the meeting room (including the first 60 s before the evacuation starts). Exposure can be divided in two phases. Phase one are the first 60 s when the persons are not moving. In this phase the exposure of a persons decreases with increasing distance to the ventilation inlets because the persons are subsequently reached by the advancing pollutant. Phase two is the evacuation phase after $t > 60$ s when the persons are moving. The persons further away from the exit have longer escape and exposure times. Thus, in phase two the exposure of a person increases with increasing escape time. It is during this phase when the persons away from the door receive most of their accumulated dose because they have to wait to pass the narrow door, where concentrations are high.

6.2. Cinema

This case is a cinema room ($27.9 \times 16.0 \times 7.9$ m) with five exits (see Fig. 10). 336 persons are seated in four blocks, each of which has seven rows with 12 seats. Pollutant is released from the back of the cinema via a jet with a diameter of 0.5 m pointing towards the screen with a speed of 15 m/s for 5 s. The evacuation starts at $t = 5$ s when the pollutant jet stops and it takes 80.5 s for all persons to leave the room.

The mesh is a Cartesian grid with a resolution of $\Delta x = 0.1$ m in the region where the persons are moving, $\Delta x = 0.05$ m around the ventilation inlets and $\Delta x = 0.2$ m in the rest of the domain, resulting in 2.6 million nodes.

The distribution of the pollutant in the cinema is shown in Fig. 11. Initially, the pollutant is concentrated in the jet. From $t = 10$ s it can be seen that air with higher pollutant concentrations is drawn in the wake of the moving persons towards the side and rear exits.

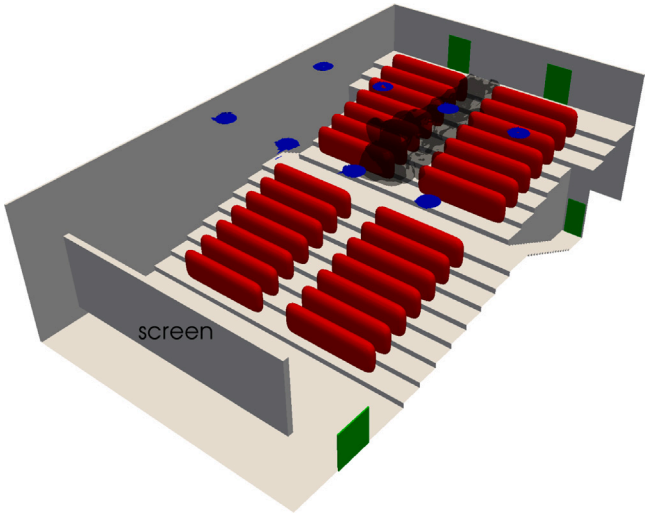

Fig. 10. The cinema with initial position of the persons (red), exits (green), ventilation inlets in the ceiling (blue) and the pollutant jet in the back (black cloud). (For interpretation of the references to color in this figure legend, the reader is referred to the web version of this article.)

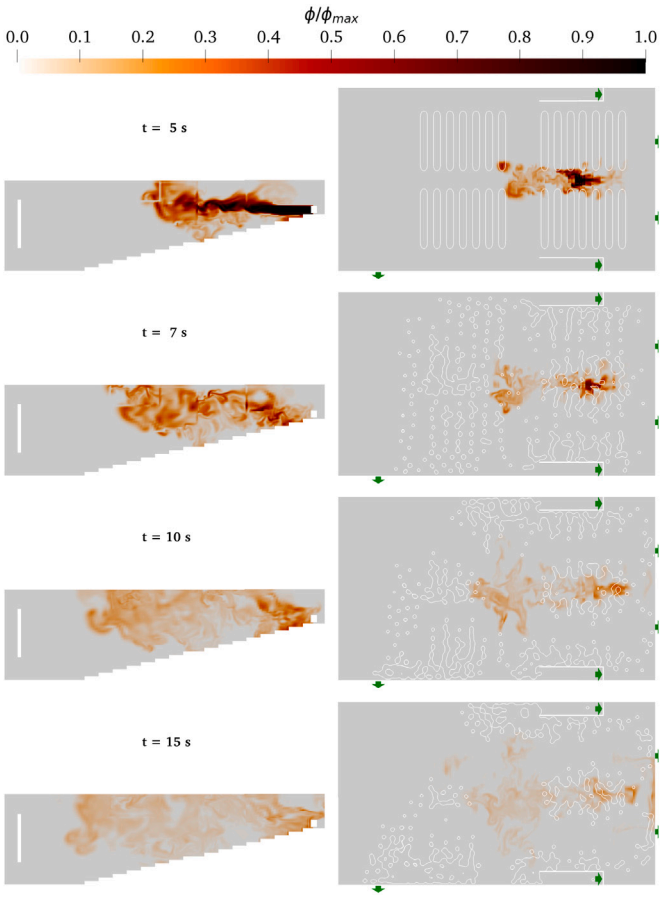

Fig. 11. Cinema: pollutant concentration in vertical center plane (left) and at head level (right, white lines indicate position of persons).

Fig. 12 shows the accumulated dose of pollutant that each person was exposed to when leaving the cinema room (including the first 5 s before the evacuation starts). The exposure strongly depends on the path a person takes. The persons leaving the cinema via the central aisle to the rear doors are exposed most because they walk directly into the

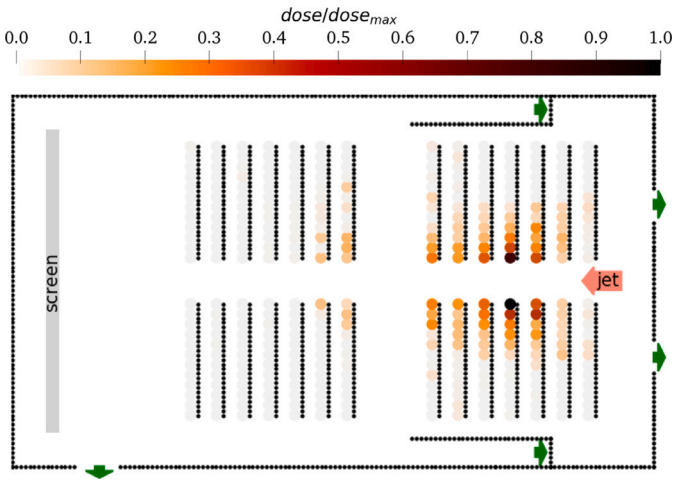

Fig. 12. Cinema: the accumulated dose of pollutant that each person is exposed to plotted on their initial position.

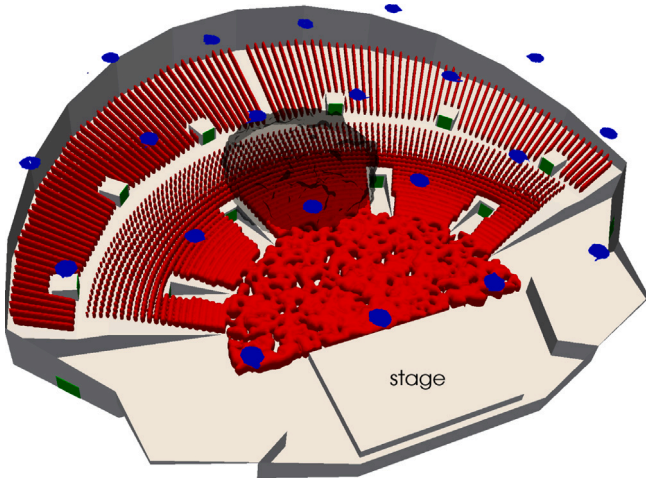

Fig. 13. The concert hall with initial position of the persons (red), exits (green), ventilation inlets in the ceiling (blue) and initial pollutant cloud in the center (black). (For interpretation of the references to color in this figure legend, the reader is referred to the web version of this article.)

pollutant jet. Just the persons in the last rows are less affected because their heads are above the jet thus avoiding high concentrations. All the persons taking another path are hardly exposed because the pollutant is not fully spread in the room by the time they leave.

6.3. Concert hall

This case is a concert hall ($83.2 \times 68.4 \times 15.1$ m) with 12 exits (see Fig. 13). It is occupied by 6026 persons of which around 2400 are standing in front of the stage and 1800 each are sitting on the lower and upper rank. The rows of seats are not explicitly modeled in the SFM, but taken into account by an obstacle factor $k_O(\mathbf{x}_i@\text{ranks}) = 0.3$ which is applied to Eq. (4) and results in a reduced walking speed on the ranks. Pollutant is instantly released from a cloud with a diameter of 20 m in the center of the concert hall. The evacuation starts immediately and it takes 299.2 s for all persons to leave the room.

The mesh is a Cartesian grid with a resolution of $\Delta x = 0.2$ m in the entire domain, resulting in 6.8 million nodes.

The distribution of the pollutant at head level in the concert hall is shown in Fig. 14. The initially emitted pollutant is drawn towards the two center exits on the upper rank by the wake of the moving persons.

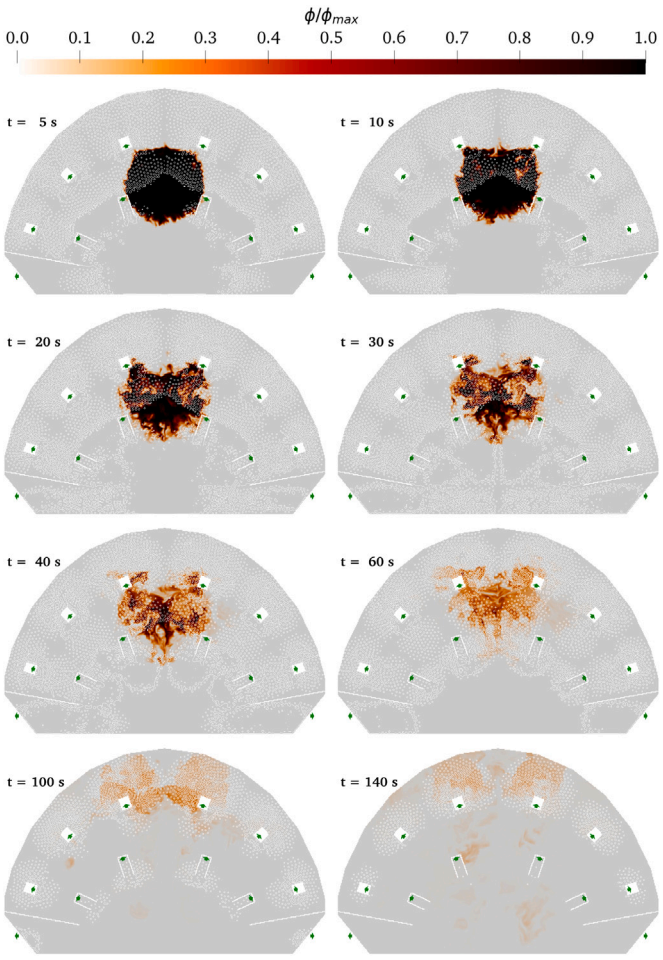

Fig. 14. Concert hall: pollutant concentration at head level (white lines indicate position of persons).

The spreading of pollutant towards the center exits on the lower rank is lesser because the persons moving this way are stuck in the queue and move very slowly. The moving persons and the complex convective flow in the concert hall result in significant pollutant concentrations at head level around the two center exits on the upper rank in the later course of the evacuation.

Fig. 15 shows the accumulated dose of pollutant that each person was exposed to when leaving the concert hall. As expected, the persons situated inside the initial pollutant cloud are strongly exposed to pollutant. Also the persons in the center of the upper rank are exposed to considerable doses because they have to wait in areas with significant pollutant concentrations, resulting in long exposure.

7. Concluding remarks

An almost unique multidisciplinary simulation tool for the simulation of pollutant dispersion under the influence of moving persons has been developed. For this purpose a human agent behavioral model, a high-fidelity lattice Boltzmann-based CFD tool and a wake model have been coupled. The behavioral model predicts evacuation path and speed of each human agent in complex environments employing a Social Force Model. The LBM Large Eddy Simulation calculates the unsteady turbulent flow dynamics and the dispersion of pollutant taking into account the influence of the human movements with the help of the wake model. The latter is realized as an Actuator Line Model that mimics the effect of moving objects by applying body forces

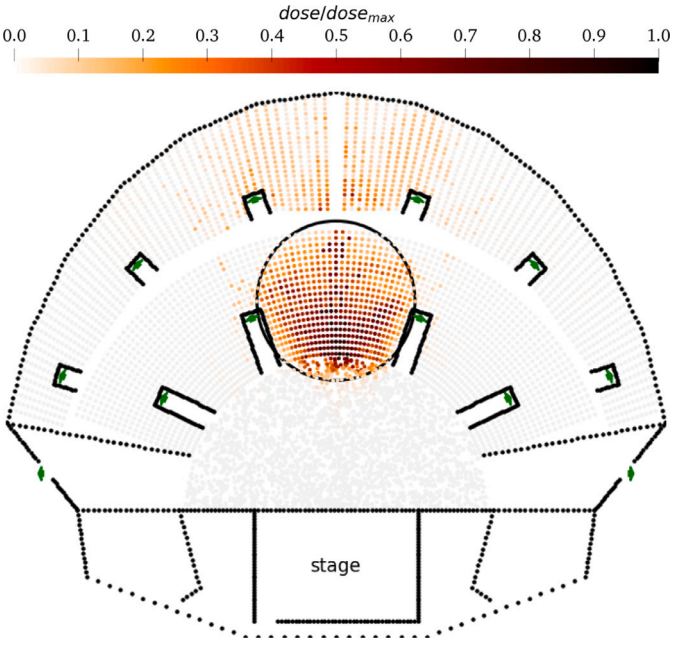

Fig. 15. Concert hall: the accumulated dose of pollutant that each person is exposed to plotted on their initial position (black circle in the center indicates position of the initial pollutant cloud).

(which represent the objects drag force) to the flow field, thus, avoiding computationally expensive dynamic meshing.

All sub-models have been validated and the capabilities of the coupled multidisciplinary model have been demonstrated at realistic full-scale evacuation scenarios with a wide range of size and occupation. A physiological model allows for a direct access to the instantaneous and time-integrated environmental parameters (pollutant concentration at head level, but also temperature) for each person during the evacuation process. This enables a detailed estimation of how much each person is exposed to the pollutant and to assess associated health risks.

Declaration of competing interest

The authors declare that they have no known competing financial interests or personal relationships that could have appeared to influence the work reported in this paper.

Acknowledgments

Many thanks to Patrick Teyou for his valuable work in the development of the Social Force Model described in Section 2.1.

Dr. Lucie Merlier from CETHIL is warmly acknowledged for designing the three room geometries presented in Section 6.

Centre de Calcul Intensif d'Aix-Marseille is acknowledged for granting access to its high performance computing resources. This work was granted access to the HPC resources of CINES under the allocation 2021-A0092A07679 made by GENCI.

References

[1] H. Liu, S. He, L. Shen, J. Hong, Simulation-based study of COVID-19 outbreak associated with air-conditioning in a restaurant, Phys. Fluids 33 (2) (2021) 023301, http://dx.doi.org/10.1063/5.0040188.

[2] F. Yang, A.A. Pahlavan, S. Mendez, M. Abkarian, H.A. Stone, Towards improved social distancing guidelines: Space and time dependence of virus transmission from speech-driven aerosol transport between two individuals, Phys. Rev. Fluids 5 (2020) 122501, http://dx.doi.org/10.1103/PhysRevFluids.5.122501.

[3] Z. Li, H. Wang, X. Zhang, T. Wu, X. Yang, Effects of space sizes on the dispersion of cough-generated droplets from a walking person, Phys. Fluids 32 (12) (2020) 121705, http://dx.doi.org/10.1063/5.0034874.

[4] C. Caliendo, P. Ciambelli, R. Del Regno, M. Meo, P. Russo, Modelling and numerical simulation of pedestrian flow evacuation from a multi-storey historical building in the event of fire applying safety engineering tools, J. Cult. Herit. 41 (2020) 188–199, http://dx.doi.org/10.1016/j.culher.2019.06.010.

[5] C. Caliendo, P. Ciambelli, R. Del Regno, M. Meo, P. Russo, Simulation of people evacuation in the event of a road tunnel fire, Procedia - Soc. Behav. Sci. 53 (2012) 178–188, http://dx.doi.org/10.1016/j.sbspro.2012.09.871.

[6] H. Cai, W. Long, X. Li, D. Barker, Evaluating emergency ventilation strategies under different contaminant source locations and evacuation modes by efficiency factor of contaminant source (EFCS), Build. Environ. 45 (2) (2010) 485–497, http://dx.doi.org/10.1016/j.buildenv.2009.07.005.

[7] J. Makmul, A pedestrians flow model during propagation of smoke: Microscopic and macroscopic approaches, Saf. Sci. 133 (2021) 105006, http://dx.doi.org/10.1016/j.ssci.2020.105006.

[8] W. Wu, Z. Lin, Experimental study of the influence of a moving manikin on temperature profile and carbon dioxide distribution under three air distribution methods, Build. Environ. 87 (2015) 142–153, http://dx.doi.org/10.1016/j.buildenv.2015.01.027.

[9] P. Kalliomäki, K. Hagström, H. Itkonen, I. Grönvall, H. Koskela, Effectiveness of directional airflow in reducing containment failures in hospital isolation rooms generated by door opening, Build. Environ. 158 (2019) 83–93, http://dx.doi.org/10.1016/j.buildenv.2019.04.034.

[10] W. Zhao, S. Lestinen, S. Kilpeläinen, R. Kosonen, An experimental study of the influence of a moving person on airflow characteristics and thermal conditions with diffuse ceiling ventilation, Indoor Built Environ. 29 (6) (2020) 860–880, http://dx.doi.org/10.1177/1420326X20917202.

[11] A. Bhattacharya, J. Pantelic, A. Ghahramani, E.S. Mousavi, Three-dimensional analysis of the effect of human movement on indoor airflow patterns, Indoor Air 31 (2) (2021) 587–601, http://dx.doi.org/10.1111/ina.12735.

[12] B.A. Edge, E.G. Paterson, G.S. Settles, Computational study of the wake and contaminant transport of a walking human, J. Fluids Eng. 127 (5) (2005) 967–977, http://dx.doi.org/10.1115/1.2013291.

[13] Y. Tao, K. Inthavong, J. Tu, A numerical investigation of wind environment around a walking human body, J. Wind Eng. Ind. Aerodyn. 168 (2017) 9–19, http://dx.doi.org/10.1016/j.jweia.2017.05.003.

[14] S.-J. Cao, D. Cen, W. Zhang, Z. Feng, Study on the impacts of human walking on indoor particles dispersion using momentum theory method, Build. Environ. 126 (2017) 195–206, http://dx.doi.org/10.1016/j.buildenv.2017.10.001.

[15] J. Choi, J. Edwards, Large eddy simulation and zonal modeling of human-induced contaminant transport, Indoor Air 18 (2008) 233–249, http://dx.doi.org/10.1111/j.1600-0668.2008.00527.x.

[16] J.N. Sørensen, W.Z. Shen, Numerical modeling of wind turbine wakes, J. Fluids Eng. 124 (2) (2002) 393–399, http://dx.doi.org/10.1115/1.1471361.

[17] N. Troldborg, Actuator Line Modeling of Wind Turbine Wakes (Ph.D. thesis), 2009.

[18] M. Churchfield, S. Lee, P. Moriarty, L. Martínez Tossas, S. Leonardi, G. Vijayakumar, J. Brasseur, A large-eddy simulation of wind-plant aerodynamics, ISBN: 978-1-60086-936-5, 2012, http://dx.doi.org/10.2514/6.2012-537.

[19] R.J. Stevens, L.A. Martínez-Tossas, C. Meneveau, Comparison of wind farm large eddy simulations using actuator disk and actuator line models with wind tunnel experiments, Renew. Energy 116 (2018) 470–478, http://dx.doi.org/10.1016/j.renene.2017.08.072.

[20] S. Rullaud, F. Blondel, M. Cathelain, Actuator-line model in a lattice Boltzmann framework for wind turbine simulations, J. Phys. Conf. Ser. 1037 (2018) 022023, http://dx.doi.org/10.1088/1742-6596/1037/2/022023.

[21] H. Asmuth, H. Olivares-Espinosa, S. Ivanell, Actuator line simulations of wind turbine wakes using the lattice Boltzmann method, Wind Energy Sci. 5 (2) (2020) 623–645, http://dx.doi.org/10.5194/wes-5-623-2020.

[22] D. Helbing, A mathematical model for the behavior of pedestrians, Behav. Sci. 36 (4) (1991) 298–310, http://dx.doi.org/10.1002/bs.3830360405.

[23] D. Helbing, P. Molnar, Social force model for pedestrian dynamics, Phys. Rev. E 51 (5) (1995) 4282–4286, http://dx.doi.org/10.1103/PhysRevE.51.4282.

[24] J.A. Sethian, A fast marching level set method for monotonically advancing fronts, Proc. Natl. Acad. Sci. 93 (4) (1996) 1591–1595.

[25] R. Kimmel, J.A. Sethian, Fast Marching Methods for Computing Distance Maps and Shortest Paths, Technical Report LBL-38451, Lawrence Berkeley Nat. Lab., Berkeley, CA, 1996.

[26] D. Helbing, I.J. Farkas, P. Molnar, T. Vicsek, Simulation of pedestrian crowds in normal and evacuation situations, in: M. Schreckenberg, S.D. Sharma (Eds.), Pedestrian and Evacuation Dynamics, Springer, Berlin, 2002, pp. 21–58, Pedestrian and Evacuation Dynamics. Conference. Duisburg, Germany. April 4–6, 2001.

[27] W. Yu, A. Johansson, Modeling crowd turbulence by many-particle simulations, Phys. Rev. E 76 (4) (2007) 046105, http://dx.doi.org/10.1103/PhysRevE.76.046105.

[28] H.L. Klüpfel, A Cellular Automaton Model for Crowd Movement and Egress Simulation (Ph.D. thesis), Universität Duisburg–Essen, Duisburg, Germany, 2003.

[29] CS, ProLB website, 2017, URL: http://www.prolb-cfd.com/.

[30] T. Krüger, H. Kusumaatmaja, A. Kuzmin, O. Shardt, G. Silva, E.M. Viggen, The Lattice Boltzmann Method: Principles and Practice, in: Graduate Texts in Physics, Springer, 2017.

[31] Z. Guo, C. Zheng, B. Shi, Discrete lattice effects on the forcing term in the lattice Boltzmann method, Phys. Rev. E 65 (4) (2002) http://dx.doi.org/10.1103/PhysRevE.65.046308.

[32] J. Jacob, O. Malaspinas, P. Sagaut, A new hybrid recursive regularised Bhatnagar–Gross–Krook collision model for Lattice Boltzmann method-based large eddy simulation, J. Turbul. (2018) 1–26, http://dx.doi.org/10.1080/14685248.2018.1540879.

[33] Y. Feng, P. Boivin, J. Jacob, P. Sagaut, Hybrid recursive regularized lattice Boltzmann simulation of humid air with application to meteorological flows, Phys. Rev. E (2019) http://dx.doi.org/10.1103/PhysRevE.100.023304.

[34] J. Jacob, P. Sagaut, Wind comfort assessment by means of large eddy simulation with lattice Boltzmann method in full scale city area, Build. Environ. 139 (2018) 110–124, http://dx.doi.org/10.1016/j.buildenv.2018.05.015.

[35] L. Merlier, J. Jacob, P. Sagaut, Lattice-Boltzmann large-eddy simulation of pollutant dispersion in street canyons including tree planting effects, Atmos. Environ. 195 (2018) 89–103, http://dx.doi.org/10.1016/j.atmosenv.2018.09.040.

[36] L. Merlier, J. Jacob, P. Sagaut, Lattice-Boltzmann large-eddy simulation of pollutant dispersion in complex urban environment with dense gas effect: Model evaluation and flow analysis, Build. Environ. 148 (2019) 634–652, http://dx.doi.org/10.1016/j.buildenv.2018.11.009.

[37] J.D. Anderson, Fundamentals of Aerodynamics, sixth ed., McGraw-Hill Education, New York, 2017.

[38] L.A. Martínez-Tossas, M.J. Churchfield, C. Meneveau, Optimal smoothing length scale for actuator line models of wind turbine blades based on Gaussian body force distribution, Wind Energy (Chichester, England) 20 (6) (2017) 1083–1096, http://dx.doi.org/10.1002/we.2081.

[39] N. Troldborg, F. Zahle, P.-E. Réthoré, N.N. Sørensen, Comparison of wind turbine wake properties in non-sheared inflow predicted by different computational fluid dynamics rotor models, Wind Energy (Chichester, England) 18 (7) (2015) 1239–1250, http://dx.doi.org/10.1002/we.1757.

[40] M. Grondeau, S. Guillou, P. Mercier, E. Poizot, Wake of a ducted vertical axis tidal turbine in turbulent flows, LBM actuator-line approach, Energies 12 (22) (2019) http://dx.doi.org/10.3390/en12224273.

[41] L. Martínez, S. Leonardi, M. Churchfield, P. Moriarty, A comparison of actuator disk and actuator line wind turbine models and best practices for their use, in: 50th AIAA Aerospace Sciences Meeting Including the New Horizons Forum and Aerospace Exposition, 2012, http://dx.doi.org/10.2514/6.2012-900.